



**HAL**  
open science

## Mapping a geothermal anomaly using apatite (U-Th)/He thermochronology in the Têt fault damage zone, eastern Pyrenees, France

Gaétan Milesi, Roger Soliva, Patrick Monie, Philippe Munch, Mathieu Bellanger, Olivier Bruguier, Michael Bonno, Audrey Taillefer, Sylvain Mayolle

### ► To cite this version:

Gaétan Milesi, Roger Soliva, Patrick Monie, Philippe Munch, Mathieu Bellanger, et al.. Mapping a geothermal anomaly using apatite (U-Th)/He thermochronology in the Têt fault damage zone, eastern Pyrenees, France. *Terra Nova*, 2019, 31 (6), pp.569-576. 10.1111/TER.12429 . hal-02909833

**HAL Id: hal-02909833**

**<https://hal.science/hal-02909833v1>**

Submitted on 31 Jul 2020

**HAL** is a multi-disciplinary open access archive for the deposit and dissemination of scientific research documents, whether they are published or not. The documents may come from teaching and research institutions in France or abroad, or from public or private research centers.

L'archive ouverte pluridisciplinaire **HAL**, est destinée au dépôt et à la diffusion de documents scientifiques de niveau recherche, publiés ou non, émanant des établissements d'enseignement et de recherche français ou étrangers, des laboratoires publics ou privés.

DR GAETAN MILESI (Orcid ID : 0000-0001-8658-9837)

Article type : Paper

## Mapping a geothermal anomaly using apatite (U-Th)/He thermochronology in the Têt fault damage zone, eastern Pyrenees, France

**Gaétan Milesi<sup>1a</sup>, Roger Soliva<sup>1b</sup>, Patrick Monié<sup>1c</sup>, Philippe Münch<sup>1d</sup>, Mathieu Bellanger<sup>2</sup>, Olivier Bruguier<sup>1e</sup>, Michael Bonno<sup>1f</sup>, Audrey Taillefer<sup>1g</sup>, and Sylvain Mayolle<sup>1h</sup>**

<sup>1</sup>Géosciences Montpellier, Université de Montpellier, CNRS, Université des Antilles, Campus Triolet, CC060, Place Eugène Bataillon, 34095 Montpellier Cedex 05, France

<sup>1a</sup> *gaetan.milesi@umontpellier.fr*

<sup>1b</sup> *roger.soliva@umontpellier.fr*

<sup>1c</sup> *patrick.monie@umontpellier.fr*

<sup>1d</sup> *philippe.munch@umontpellier.fr*

<sup>1e</sup> *olivier.bruguier@umontpellier.fr*

<sup>1f</sup> *michael.bonno@umontpellier.fr*

<sup>1g</sup> *audrey.taillefer@gmail.com*

<sup>1h</sup> *sylvain.mayolle@umontpellier.fr*

<sup>2</sup>TLS Geothermics, 92 chemin gabardie, 31200 Toulouse, France. *mathieu.bellanger@tls-geothermics.fr*

Correspondence to: Gaétan Milesi, Géosciences Montpellier, Université de Montpellier, CNRS, Université des Antilles, Campus Triolet, CC060, Place Eugène Bataillon, 34095 Montpellier Cedex 05, France (*gaetan.milesi@umontpellier.fr*).

This article has been accepted for publication and undergone full peer review but has not been through the copyediting, typesetting, pagination and proofreading process, which may lead to differences between this version and the [Version of Record](#). Please cite this article as [doi: 10.1111/TER.12429](https://doi.org/10.1111/TER.12429)

This article is protected by copyright. All rights reserved

## ABSTRACT

(U-Th)/He ages on apatite obtained in the vicinity of the Têt fault hydrothermal system show a large variability. In the inner damage zone adjacent to the fault core, where fluid flows are concentrated, AHe ages display a large scatter (3 to 41 Ma) and apatite ageing. Samples from the outer damage zone show young ages with less dispersion (0.9 to 21.1 Ma) and apatite rejuvenation. Outside the damage zone, ages are consistent with the regional exhumation history between 20 and 12 Ma. The important age dispersion found in the damage zone is interpreted as the result of  $^4\text{He}$  mobility during fluid infiltration. Our results show that thermochronological data close to a fault should be interpreted with caution, but may offer a new tool for geothermal exploration.

## INTRODUCTION

Low temperature (U-Th)/He thermochronology is commonly used to investigate exhumation and thermal evolution of mountain belts. Few studies have so far been dedicated to the impact of hydrothermal activity on thermochronology (e.g. Forster and Smith, 1989; Deming, 1994) and more particularly on the behaviour of apatite in geothermal systems (Duddy et al., 1998; Whipp and Ehlers, 2007; Wölfler et al., 2010; Luijendijk, 2012; Gorynski et al., 2014; Hickey et al., 2014; Valla et al., 2016). Meteoric fluids infiltrated from reliefs adjacent to faults generate subsurface thermal anomalies along the fault during their upflow (McKenna and Blackwell, 2004). Significant geothermal anomalies (up to  $90^\circ\text{C}/\text{km}$ ) are interpreted as resulting from the combination of three main factors, (1) high rock permeability, (2) substantial adjacent topography and (3) prolonged fault activity, which may transport rock and heat from depth and also generate frictional heat (Saffer et al., 2003; Sutherland et al., 2017, Jordan et al., 2018). Even for a weakly active fault but adjacent to high relief (about 1.5 km escarpment), a geothermal loop can be active over a period  $>10^6$  year (Taillefer et al., 2018).

In this study, we evaluate the impact of hydrothermal flow on apatite (U-Th)/He (AHe) ages from the Têt Fault damage zone (DZ) which presently undergoes important hydrothermal activity. We mapped the fracture frequency distribution near the Têt fault and measured He ages of apatites from

both in and outside the DZ. We discuss the impact of fluid-rock interaction and a localized thermal anomaly on AHe age dispersion.

## **GEOLOGICAL SETTING**

The Têt normal fault is a 100 km long, north dipping crustal-scale structure striking WSW-ENE (Fig. 1). In the study area, the fault crosscuts Palaeozoic magmatic and metamorphic rocks of the Mont Louis, Canigou and Carança massifs. Periods of tectonic activity resulted in ~2000 m of footwall uplift of the Canigou massif between 21 and 18 Ma (Maurel et al., 2008) in response to the Gulf of Lion rifting (Séranne et al., 1995). Late Miocene to Pliocene tectonic activity is limited to a maximum of 300 m footwall uplift and moderate dextral strike-slip (e.g. Cabrera et al., 1988; Mauffret et al., 2001). The amplitude of Pliocene to Quaternary activity is minor and still debated (see discussion in e.g. Carozza and Baize, 2004; Lacan and Ortuño, 2012; Petit and Mouthereau, 2012)

In the Canigou massif, erosion is constrained by low temperature thermochronology showing erosion rates of about 100 m/m.y. and a mean cooling rate of 3°C/m.y. during the Middle-Late Miocene (Maurel et al. 2008). For the Têt valley low incision rates between 1 and 25 m/m.y. since 6 Ma have been estimated by cosmogenic nuclides (Delmas et al., 2018; Sartégou et al., 2018) indicate lower incision rates between 1 and 25m/m.y.

29 hot springs distributed in 4 main clusters are localised along the weakly active Têt fault (Souriau and Pauchet, 1998) (Appendix 1.1). These springs are essentially located in the highly permeable DZ (Taillefer et al., 2017). Due to the presence of low-permeable metasediments in the hanging wall, fluid infiltration is mainly concentrated in the DZ of the footwall. Taillefer et al. (2017) proposed that the present-day hydrothermal disturbance of the geotherm vanishes at about 300m away from the fault. In this study, we focused on the main hot spring cluster near Thuès-les-Bains (Fig. 1) showing water temperatures up to 75°C.

## **SAMPLING AND ANALYTICAL METHODS**

First, we studied the fracture distribution in the Têt fault footwall by measuring the frequency and the strike orientation of silica and carbonate colloids filled fractures, attributed to combined

tectonic and hydrothermal activity (Taillefer et al., 2017), along a 500 m long profile perpendicular to the fault (Fig. 1).

To study the influence of hydrothermal springs on AHe thermochronometer, nine Palaeozoic gneisses were sampled (Appendix 1.2) and yielded 48 AHe ages. Samples TET1 to TET4 are located along a profile nearly perpendicular to the Têt fault, TET5 is located to the southwest and TET6 and TET7 to the east of the profile. TET1, adjacent to the fault core, is highly fractured, chloritised and hydrothermalised. TET6 occupies the same structural setting as TET1 while TET7 belongs to a subsidiary branch of the main fault. Sampling covers an elevation range of 1100 m.

Single apatite crystals have been analysed for AHe dating following the procedure described in Wu et al., (2016). For each sample, three to ten inclusion- and fracture-free crystals were dated (Appendix 1.3). REE concentrations have additionally been determined for the grains of four dated samples (TET1, TET1.1, TET2.1 and TET5) following the procedure described in Bruguier et al. (2003). Microprobe analyses were also performed to evaluate the chlorine content of apatite grains (Appendix 2.1).

## RESULTS

The frequency of fractures crosscutting the Palaeozoic foliation shows an approximate logarithmic decrease, formed of small modes due to secondary faults, similarly to the classic fracture patterns observed in fault DZ elsewhere. Fault zone domains (Fig. 2) are defined according to the Choi et al. (2016) cumulative fracture method (Appendix 1.4). Silica filled fractures are mainly sub-vertical (i.e. some of them dip slightly to the North) and their strike is mainly NE-SW, i.e. consistent with the regional extension, and oblique to the Têt fault in the study area (red star in Fig. 2b). Carbonate filled fractures often crosscut silica filled ones. They show more variable orientations but also a well expressed cluster of trend kinematically consistent with the local trend of the Têt fault (Taillefer et al., 2017).

All dated samples are shown on a cross section in Figure 3. Single grain AHe ages are reported on Figure 4a with respect to fault distance and to the defined fault (Appendix 2.2). Samples TET1 and TET6 from the inner DZ display a large scatter of single grain ages between 41 Ma and 3 Ma, with 11 ages among 14 in the range of 22-41 Ma and with eU values <25 ppm (Appendix 2.3). In the outer

DZ, samples TET1.1, TET2 and TET2.1 show less dispersion between 0.9 Ma to 21.1 Ma with 10 among 16 apatites younger than 6 Ma. Outside the DZ, three samples (TET3, TET4 and TET7) give mean AHe ages respectively of  $11.7\pm 0.8$  Ma,  $13.7\pm 0.5$  Ma and  $13.4\pm 0.8$  Ma. At 3700 m from the fault, AHe ages from site TET5 (mean:  $20.4\pm 1.2$  Ma) are in the range of AHe ages obtained by Maurel et al. (2008) in the Canigou massif. An age-elevation relationship can be defined only with samples outside the DZ that indicate a mean exhumation rate of about 65 m/m.y. between 12 and 20 Ma (Fig. 4b). With respect to this age-elevation relationship, samples from the outer DZ show anomalously young and dispersed ages, whereas in the inner DZ, samples show mostly anomalously old and even more dispersed ages, with the exception of two grains at  $4.0\pm 0.2$  Ma and  $2.7\pm 0.3$  Ma. Microprobe and SEM analyses indicate that all analysed apatites are fluorapatites homogeneous in composition and poor in chlorine (Appendix 1.3 and 2.1) suggesting no compositional influence on this age dispersion (Gautheron et al., 2013).

We measured the REE content of the dated apatite grains from the DZ samples TET1, TET1.1 and TET2.1, and also from sample TET5 far from the fault zone as a reference for the protolith unaffected by hydrothermal circulation (Fig. 4c). All REE patterns (normalised to chondrite values, Sun and McDonough, 1989) display the common profile of granitic lithologies (Sha and Chappell, 1999), indicating that the analysed apatites are cogenetic (Fig. 4c). Note that apatites from the outer DZ (TET1.1 and TET2.1) that mainly display young ages show low REE contents with respect to TET5, whereas apatites from the inner DZ mainly displaying old ages (TET1) have slightly higher REE contents

## DISCUSSION

AHe ages reflect the time at which a rock passes through the partial retention zone (PRZ), which lies between  $90^{\circ}\text{C}$  and  $30^{\circ}\text{C}$  (Gautheron et al., 2009; Shuster and Farley, 2009). Thermal numerical modelling using QTQt (Gallagher, 2012) for samples outside the DZ points to a rapid cooling of  $\sim 24^{\circ}\text{C}/\text{m.y.}$  between 30 and 24 Ma followed by constant cooling of  $3^{\circ}\text{C}/\text{m.y.}$  since 24 Ma (Fig. 5; Appendix 3.1 for inputs in the model). This thermal history is consistent with that obtained for the Canigou massif by Maurel et al. (2008) for the same period.

In the DZ, apatites show a larger scatter of AHe ages (1 to 41 Ma) and an important variability of their REE content with respect to the reference sample TET5. Young apatites are depleted in REE, whereas old apatites have slightly enriched REE patterns. Such REE mobility in apatite has already been mentioned by Harlov (2015) and it is likely that U and Th behave similarly due to related theoretical solubilities with REE (Cramer and Nesbitt, 1983; Gieré, 1990). This REE depletion therefore suggests that apatites from the DZ may behave as open systems during interaction with hydrothermal fluids.

Young ages <6 Ma, mainly from the outer DZ, might be explained by different effects. A renewed recent footwall uplift and progressive crossing of the PRZ cannot explain these young ages that do not fit with predicted ages using QTQt thermal modelling (Appendix 3.2). Rejuvenation of the AHe ages can result only from thermal resetting and coeval He loss triggered by hydrothermal heat advection within the DZ. As a first proxy, the conditions of this resetting have been estimated with HeFty models using the diffusion model of Farley (2000) (Appendix 3.3). The favoured thermal models suggest that temperatures needed to rejuvenate apatites lie between 60°C and 90°C assuming a stable heating duration of less than 6 Ma in accordance with the proposal by Taillefer et al. (2017). However, since apatites in the outer DZ show REE mobility, it is likely that thermal diffusion was not the only cause of apatite rejuvenation. We cannot exclude that this REE behaviour was coupled with some uranium and thorium mobility, as suggested by the isotopic data in a ternary U-Th-He plot (Fig. 6). Although in such ternary plot the data might be interpreted as U gain, the hypothesis would imply that U mobility behaved in the opposite way than the REE, which is inconsistent with their close theoretical solubilities. Therefore, we propose that the He loss enhanced by thermal diffusion mainly account for the observed AHe ages rejuvenation.

Old AHe ages, mainly from the highly hydrothermalised inner DZ, show a large age dispersion between 22 and 41 Ma and are older than AHe ages outside the damage zone even at higher elevations. Such old and scattered ages cannot be reproduced by any diffusion model (Flowers et al., 2009; Gautheron et al., 2009; Appendix 3.2) thus another mechanism for apatite ageing has been suggested (Green and Duddy, 2018). U and Th mobility cannot account for the old AHe ages (Fig. 6) as we observed slightly enriched REE patterns (Fig. 4c) that could lead to a gain of parent isotopes and thus a rejuvenation of ages. The alternative process would be an excess of He that may

be related to either He implantation from grain boundary phases (oxides, Murray et al., 2014) or neighbouring U-rich grains (e.g. zircon, Gautheron et al., 2012), or grain shape effects (broken grains, Brown et al., 2013) or He trapping within lattice defects (Zeitler et al., 2017) or U-rich inclusions (Vermeesch et al., 2007). Because of the lack of oxides covering the surfaces of the dated apatite grains and the scarcity of U-rich minerals within the studied gneisses, direct He implantation seems unlikely (Appendix 1.3). In the same way, broken grain effects cannot account for the observed magnitude of age dispersion (400%) and U-rich inclusions have not been detected by SEM imaging (Appendix 1.3), even if this effect cannot be completely ruled out as the polished apatite used for imaging cannot be used for AHe dating. We propose that old (22-41 Ma) apatite grains were contaminated by He released at higher depth and carried by hydrothermal fluids, which also induce REE mobility. This is supported by the occurrence of  $^4\text{He}$  rich hydrothermal fluids circulating along fault systems within granitic basement geothermal fields (Paternoster et al., 2017; Jiang et al., 2018). In such a setting, the  $^3\text{He}/^4\text{He}$  ratio is much lower than in air-saturated waters or in the mantle thus indicating that  $^4\text{He}$  is mainly radiogenic and derived from the decay of U and Th in the granitic crust. Such excess He may be hosted by fluid inclusions or by micro- to nanovoids filling within the apatite lattice following the mechanism proposed by Zeitler et al. (2017).

In the DZ, the dispersion of AHe ages may reflect the heterogeneous impact of fluid flow into naturally fractured rocks (Bense et al., 2013) at outcrop or hand specimen scale. In the same sample, apatite along fractures may exchange chemical elements with hydrothermal fluids (taking up He), while those in textural domains preserved from fracturing and fluid flow may lose radiogenic He by thermal diffusion due to heat advected by external fluids. Channelized fluid upflow through the DZ may also account for the observed difference between the outer and inner DZ, as  $^4\text{He}$  rich fluids may have been restricted to the inner DZ, in the vicinity of paleo-hot springs. We propose that the mobility of  $^4\text{He}$  (Fig. 6) associated to hydrothermal fluid circulations may drastically impact AHe thermochronometry around faults.

## CONCLUSION

The Têt normal fault hydrothermal system shows a large dispersion of AHe ages within the DZ and allows demonstrating the effects of an actual geothermal system on thermochronological



records. AHe ages away from the DZ are consistent with the regional cooling and tectonic uplift in Miocene times. Two domains are distinguished within the DZ based on fracture analysis. In both domains apatites seem to behave as open systems in response to interactions with hydrothermal fluids, which is supported by REE mobility and AHe dispersion. Differences between the outer and inner DZ (Fig. 6) are likely caused by an increase of fluid flow toward the inner DZ. In the outer DZ, apatites may be affected by heterogeneous degrees of He loss triggering a partial rejuvenation of AHe ages. In the inner DZ, apatites may be mostly affected by He trapping responsible for an increase of the AHe ages. Consequently, AHe ages from these two domains within the DZ of the Têt fault cannot be used to constrain tectonic uplift.

These conclusions suggest that AHe ages provided by samples collected next to large fault damage zones must be interpreted with caution, since actual or paleo-hydrothermal activity, or fluid flow in general, might have taken place and modified the He content in apatite. In contrast, however, these results open new perspectives for geothermal exploration along faults adjacent to high relief.

#### **ACKNOWLEDGMENTS**

This work was funded by THERMOFAULT, a project supported by the Region Occitanie (France) involving TLS Geothermics (main sponsor), Géosciences Montpellier and the TelluS Program of CNRS/INSU. Thanks to Céline Martin and Cyprien Astoury for their technical support. Thanks to Klaus Mezger, Elco Luijendijk, Mauricio Parra and an anonymous reviewer for constructive comments.

#### **REFERENCES**

- Bense, V.F., Gleeson, T., Loveless, S.E., Bour, O. and Scibek, J., 2013. Fault zone hydrogeology: *Earth-Science Reviews*, 127, p. 171–192, doi: 10.1016/j.earscirev.2013.09.008.
- Brown, R.W., Beucher, R., Roper, S., Persano, C., Stuart, F. and Fitzgerald, P., 2013. Natural age dispersion arising from the analysis of broken crystals. Part I: Theoretical basis and implications for the apatite (U–Th)/He thermochronometer: *Geochimica et Cosmochimica Acta*, 122, p. 478–497, doi: 10.1016/j.gca.2013.05.041.

Bruguier, O., Becq-Giraudon, J.F., Champenois, M., Deloule, E., Ludden, J. and Mangin, D., 2003. Application of in situ zircon geochronology and accessory phase chemistry to constraining basin development during post-collisional extension: a case study from the French Massif Central: *Chemical Geology*, 201, p. 319–336, doi: 10.1016/j.chemgeo.2003.08.005.

Cabrera, L., Roca, E. and Santanach, P., 1988. Basin formation at the end of a strike-slip fault: the Cerdanya Basin (eastern Pyrenees): *Journal of the Geological Society*, 145, p. 261–268.

Carozza, J.-M. and Baize, S., 2004. L'escarpement de faille de la Têt est-il le résultat de la tectonique active Plio-Pléistocène ou d'une exhumation Pléistocène ? *Comptes Rendus Geoscience*, 336, p. 217–226, doi: 10.1016/j.crte.2003.10.026.

Choi, J.-H., Edwards, P., Ko, K. and Kim, Y.-S., 2016. Definition and classification of fault damage zones: A review and a new methodological approach: *Earth-Science Reviews*, 152, p. 70–87, doi: 10.1016/j.earscirev.2015.11.006.

Cramer, J.J. and Nesbitt, H.W., 1983. Mass-balance relations and trace-element mobility during continental weathering of various igneous rocks: *Sciences Géologiques, bulletins et mémoires*, 73(1), p. 63–73.

Delmas, M., Calvet, M., Gunnell, Y., Voinchet, P., Manel, C., Braucher, R., Tissoux, H., Bahain, J.-J., Perrenoud, C. and Saos, T., 2018. Terrestrial  $^{10}\text{Be}$  and electron spin resonance dating of fluvial terraces quantifies quaternary tectonic uplift gradients in the eastern Pyrenees: *Quaternary Science Reviews*, 193, p. 188–211, doi: 10.1016/j.quascirev.2018.06.001.

Deming, D., 1994. Fluid flow and heat transport in the upper continental crust: Geological Society, London, Special Publications, 78, p. 27–42, doi: 10.1144/GSL.SP.1994.078.01.04.

Duddy, I.R., Green, P.F., Hegarty, K.A., Bray, R.J. and O'Brien, G.W., 1998. Dating and duration of hot fluid flow events determined using AFTA® and vitrinite reflectance-based thermal history reconstruction: Geological Society, London, Special Publications, 144, p. 41–51, doi:

10.1144/GSL.SP.1998.144.01.04.

Farley, K.A., 2000. Helium diffusion from apatite: General behavior as illustrated by Durango fluorapatite: *Journal of Geophysical Research: Solid Earth*, 105, p. 2903–2914, doi:

10.1029/1999JB900348.

Flowers, R.M., Ketcham, R.A., Shuster, D.L. and Farley, K.A., 2009. Apatite (U–Th)/He thermochronometry using a radiation damage accumulation and annealing model: *Geochimica et Cosmochimica Acta*, 73, p. 2347–2365, doi: 10.1016/j.gca.2009.01.015.

Forster, C. and Smith, L., 1989. The influence of groundwater flow on thermal regimes in mountainous terrain: A model study: *Journal of Geophysical Research*, 94, p. 9439, doi:

10.1029/JB094iB07p09439.

Gallagher, K., 2012. Transdimensional inverse thermal history modeling for quantitative thermochronology: *Journal of Geophysical Research: Solid Earth*, 117, p. n/a-n/a, doi:

10.1029/2011JB008825.

Gautheron, C., Barbarand, J., Ketcham, R.A., Tassan-Got, L., van der Beek, P., Pagel, M., Pinna-Jamme, R., Couffignal, F. and Fialin, M., 2013. Chemical influence on  $\alpha$ -recoil damage annealing in apatite: Implications for (U–Th)/He dating: *Chemical Geology*, 351, p. 257–267, doi:

10.1016/j.chemgeo.2013.05.027.

Gautheron, C., Tassan-Got, L., Ketcham, R.A. and Dobson, K.J., 2012. Accounting for long alpha-particle stopping distances in (U–Th–Sm)/He geochronology: 3D modeling of diffusion, zoning,

implantation, and abrasion: *Geochimica et Cosmochimica Acta*, 96, p. 44–56, doi: 10.1016/j.gca.2012.08.016.

Gautheron, C., Tassan-Got, L., Barbarand, J. and Pagel, M., 2009. Effect of alpha-damage annealing on apatite (U–Th)/He thermochronology: *Chemical Geology*, 266, p. 157–170, doi: 10.1016/j.chemgeo.2009.06.001.

Gieré, R., 1990. Hydrothermal mobility of Ti, Zr and REE: examples from the Bergell and Adamello contact aureoles (Italy): *Terra Nova*, 2, p. 60–67, doi: 10.1111/j.1365-3121.1990.tb00037.x.

Gorynski, K.E., Walker, J.D., Stockli, D.F. and Sabin, A., 2014. Apatite (U–Th)/He thermochronometry as an innovative geothermal exploration tool: A case study from the southern Wassuk Range, Nevada: *Journal of Volcanology and Geothermal Research*, 270, p. 99–114, doi: 10.1016/j.jvolgeores.2013.11.018.

Green, P. and Duddy, I., 2018. Apatite (U–Th–Sm)/He thermochronology on the wrong side of the tracks: *Chemical Geology*, 488, p. 21–33, doi: 10.1016/j.chemgeo.2018.04.028.

Harlov, D.E., 2015. Apatite: A Fingerprint for Metasomatic Processes: *Elements*, 11, p. 171–176, doi: 10.2113/gselements.11.3.171.

Hickey, K.A., Barker, S.L.L., Dipple, G.M., Arehart, G.B. and Donelick, R.A., 2014. The Brevity of Hydrothermal Fluid Flow Revealed by Thermal Halos around Giant Gold Deposits: Implications for Carlin-Type Gold Systems: *Economic Geology*, 109, p. 1461–1487, doi: 10.2113/econgeo.109.5.1461.

Jiang, Z., Xu, T., Owen, D.D.R., Jia, X., Feng, B. and Zhang, Y., 2018. Geothermal fluid circulation in the Guide Basin of the northeastern Tibetan Plateau: Isotopic analysis and numerical modeling: *Geothermics*, 71, p. 234–244, doi: 10.1016/j.geothermics.2017.10.007.

Jordan, T.A., Martin, C., Ferraccioli, F., Matsuoka, K., Corr, H., Forsberg, R., Olesen, A. and Siegert, M., 2018. Anomalously high geothermal flux near the South Pole: *Scientific Reports*, 8, doi: 10.1038/s41598-018-35182-0.

Lacan, P. and Ortuño, M., 2012. Active Tectonics of the Pyrenees: A review: *Journal of Iberian Geology*, 38, doi: 10.5209/rev\_JIGE.2012.v38.n1.39203.

Luijendijk, E., 2012. The role of fluid flow in the thermal history of sedimentary basins: Inferences from thermochronology and numerical modeling in the Roer Valley Graben, southern Netherlands. [PhD Thesis]: Vrije Universiteit Amsterdam, 198 p.

Mauffret, A., de Grossouvre, B.D., Dos Reis, A.T., Gorini, C. and Nercessian, A., 2001. Structural geometry in the eastern Pyrenees and western Gulf of Lion (Western Mediterranean): *Journal of Structural Geology*, 23, p. 1701–1726.

Maurel, O., Monié, P., Pik, R., Arnaud, N., Brunel, M. and Jolivet, M., 2008. The Meso-Cenozoic thermo-tectonic evolution of the Eastern Pyrenees: an  $^{40}\text{Ar}/^{39}\text{Ar}$  fission track and (U–Th)/He thermochronological study of the Canigou and Mont-Louis massifs: *International Journal of Earth Sciences*, 97, p. 565–584, doi: 10.1007/s00531-007-0179-x.

McKenna, J.R. and Blackwell, D.D., 2004. Numerical modeling of transient Basin and Range extensional geothermal systems: *Geothermics*, 33, p. 457–476, doi: 10.1016/j.geothermics.2003.10.001.

Murray, K.E., Orme, D.A. and Reiners, P.W., 2014. Effects of U–Th-rich grain boundary phases on apatite helium ages: *Chemical Geology*, 390, p. 135–151, doi: 10.1016/j.chemgeo.2014.09.023.

Paternoster, M., Oggiano, G., Sinisi, R., Caracausi, A. and Mongelli, G., 2017. Geochemistry of two contrasting deep fluids in the Sardinia microplate (western Mediterranean): Relationships with tectonics and heat sources: *Journal of Volcanology and Geothermal Research*, 336, p. 108–117, doi: 10.1016/j.jvolgeores.2017.02.011.

Petit, C. and Mouthereau, F., 2012. Steep topographic slope preservation by anisotropic diffusion: An example from the Neogene Têt fault scarp, eastern Pyrenees: *Geomorphology*, 171–172, p. 173–179, doi: 10.1016/j.geomorph.2012.05.016.

Saffer, D.M., Bekins, B.A. and Hickman, S., 2003. Topographically driven groundwater flow and the San Andreas heat flow paradox revisited: *Journal of Geophysical Research: Solid Earth*, 108(B5), doi: 10.1029/2002JB001849.

Sartégou, A., Bourlès, D.L., Blard, P.-H., Braucher, R., Tibari, B., Zimmermann, L., Leanni, L., Aumaître, G. and Keddadouche, K., 2018. Deciphering landscape evolution with karstic networks: A Pyrenean case study: *Quaternary Geochronology*, 43, p. 12–29, doi: 10.1016/j.quageo.2017.09.005.

Séranne, M., Benedicto, A., Labaum, P., Truffert, C. and Pascal, G., 1995. Structural style and evolution of the Gulf of Lion Oligo-Miocene rifting: Role of the Pyrenean orogeny: *Marine and Petroleum geology*, 12, p. 809–820.

Sha, L.-K. and Chappell, B.W., 1999. Apatite chemical composition, determined by electron microprobe and laser-ablation inductively coupled plasma mass spectrometry, as a probe into granite petrogenesis: *Geochimica et Cosmochimica Acta*, 63, p. 3861–3881, doi: 10.1016/S0016-7037(99)00210-0.

Shuster, D.L. and Farley, K.A., 2009. The influence of artificial radiation damage and thermal annealing on helium diffusion kinetics in apatite: *Geochimica et Cosmochimica Acta*, 73, p. 183–196, doi: 10.1016/j.gca.2008.10.013.

Souriau, A. and Pauchet, H., 1998. A new synthesis of Pyrenean seismicity and its tectonic implications: *Tectonophysics*, 290, p. 221–244, doi: 10.1016/S0040-1951(98)00017-1.

Sun, S.S. and McDonough, W.F., 1989. Chemical and isotopic systematics of oceanic basalts: implications for mantle composition and processes: Geological Society, London, Special Publications, 42, p. 313–345, doi: 10.1144/GSL.SP.1989.042.01.19.

Sutherland, R., Townend, J., Toy, V., Upton, P., Coussens, J., Allen, M., Baratin, L.-M., Barth, N., Becroft, L., Boese, C., Boles, A., Boulton, C., Broderick, N.G.R., Janku-Capova, L., Carpenter, B.M., Célérier, B., Chamberlain, C., Cooper, A., Coutts, A., Cox, S., Craw, L., Doan, M.-L., Eccles, J., Faulkner, D., Grieve, J., Grochowski, J., Gulley, A., Hartog, A., Howarth, J., Jacobs, K., Jeppson, T., Kato, N., Keys, S., Kirilova, M., Kometani, Y., Langridge, R., Lin, W., Little, T., Lukacs, A., Mallyon, D., Mariani, E., Massiot, C., Mathewson, L., Melosh, B., Menzies, C., Moore, J., Morales, L., Morgan, C., Mori, H., Niemeijer, A., Nishikawa, O., Prior, D., Sauer, K., Savage, M., Schleicher, A., Schmitt, D.R., Shigematsu, N., Taylor-Offord, S., Teagle, D., Tobin, H., Valdez, R., Weaver, K., Wiersberg, T., Williams, J., Woodman, N. and Zimmer, M., 2017. Extreme hydrothermal conditions at an active plate-bounding fault: *Nature*, 546, p. 137–140, doi: 10.1038/nature22355.

Taillefer, A., Guillou-Frottier, L., Soliva, R., Magri, F., Lopez, S., Courrioux, G., Millot, R., Ladouche, B. and Le Goff, E., 2018. Topographic and Faults Control of Hydrothermal Circulation Along Dormant Faults in an Orogen: *Geochemistry, Geophysics, Geosystems*, doi: 10.1029/2018GC007965.

Taillefer, A., Soliva, R., Guillou-Frottier, L., Le Goff, E., Martin, G. and Séranne, M., 2017. Fault-Related Controls on Upward Hydrothermal Flow: An Integrated Geological Study of the Têt Fault System, Eastern Pyrénées (France): *Geofluids*, 2017, p. 1–19, doi: 10.1155/2017/8190109.

Valla, P.G., Rahn, M., Shuster, D.L. and van der Beek, P.A., 2016. Multi-phase late-Neogene exhumation history of the Aar massif, Swiss central Alps: *Terra Nova*, 28, p. 383–393, doi: 10.1111/ter.12231.

Vermeesch, P., 2010. HelioPlot, and the treatment of overdispersed (U–Th–Sm)/He data: *Chemical Geology*, 271, p. 108–111, doi: 10.1016/j.chemgeo.2010.01.002.

Vermeesch, P., Seward, D., Latkoczy, C., Wipf, M., Günther, D. and Baur, H., 2007.  $\alpha$ -Emitting mineral inclusions in apatite, their effect on (U–Th)/He ages, and how to reduce it: *Geochimica et Cosmochimica Acta*, 71, p. 1737–1746, doi: 10.1016/j.gca.2006.09.020.

Whipp, D.M. and Ehlers, T.A., 2007. Influence of groundwater flow on thermochronometer-derived exhumation rates in the central Nepalese Himalaya: *Geology*, 35, p. 851, doi: 10.1130/G23788A.1.

Wölfler, A., Kurz, W., Danišík, M. and Rabitsch, R., 2010. Dating of fault zone activity by apatite fission track and apatite (U–Th)/He thermochronometry: a case study from the Lavanttal fault system (Eastern Alps): *Dating of fault zone activity: Terra Nova*, p. no-no, doi: 10.1111/j.1365-3121.2010.00943.x.

Wu, L., Monié, P., Wang, F., Lin, W., Ji, W., Bonno, M., Münch, P. and Wang, Q., 2016. Cenozoic exhumation history of Sulu terrane: Implications from (U–Th)/He thermochronology: *Tectonophysics*, 672–673, p. 1–15, doi: 10.1016/j.tecto.2016.01.035.

Zeitler, P.K., Enkelmann, E., Thomas, J.B., Watson, E.B., Ancuta, L.D. and Idleman, B.D., 2017. Solubility and trapping of helium in apatite: *Geochimica et Cosmochimica Acta*, 209, p. 1–8, doi: 10.1016/j.gca.2017.03.041.

Additional supporting information may be found online in the Appendix section.



## FIGURE CAPTIONS

Figure 1. a) Location of the study area at the scale of the Mediterranean Sea and a regional map with outline of study area and location of sample profile by Maurel et al. (2008). b) Geologic map of the hydrothermally active Têt fault near Thuès-Entre-Valls, southern France. Hot springs are indicated by dots with colours referring to spring water temperatures (modified from Taillefer et al., 2017). Sampling sites are indicated by stars. Black line near Thuès-Entre-Valls shows scan line location of figure 3.

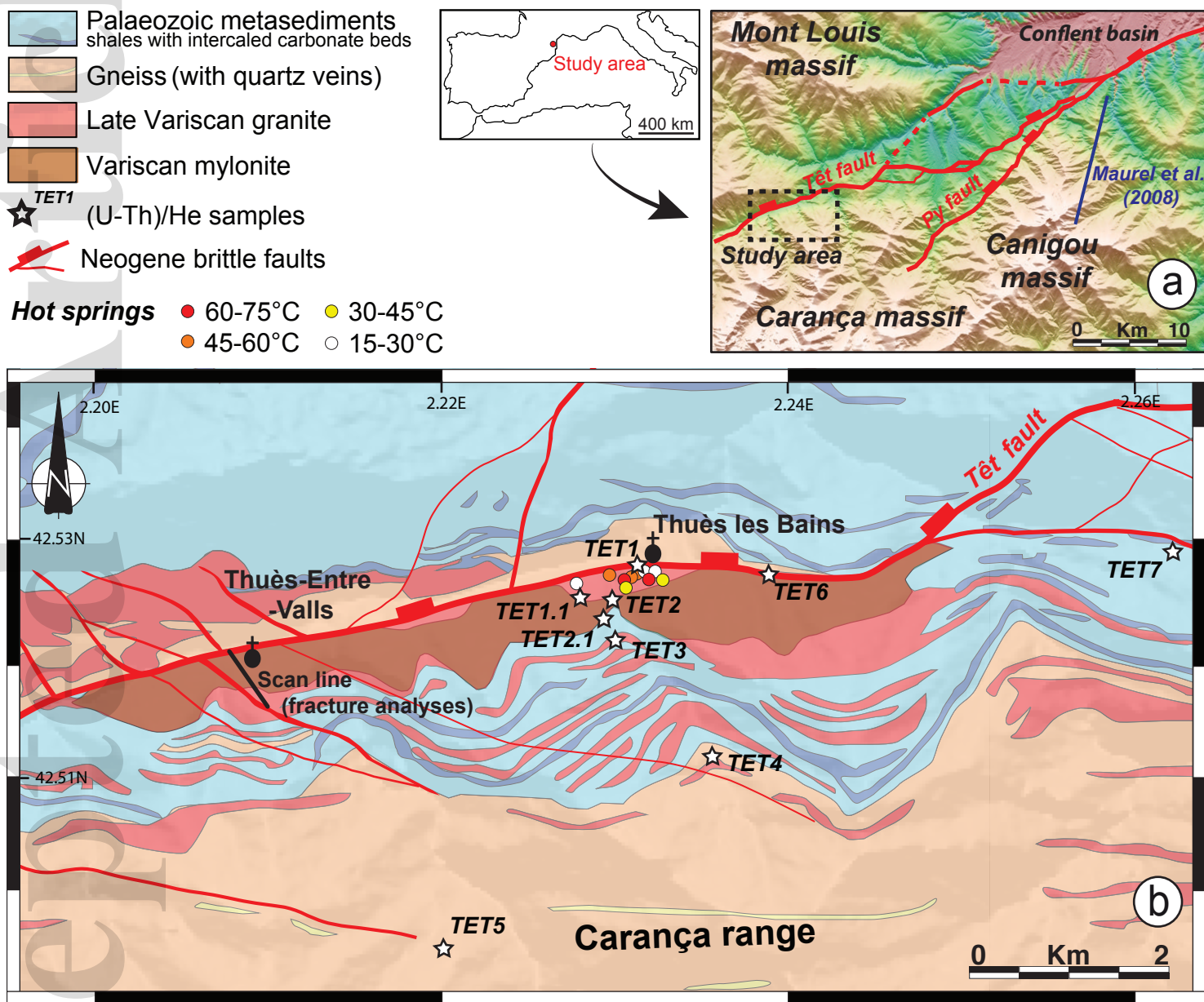
Figure 2. a) Histogram showing the number of mineralised fractures as a function of normal distance from the Têt fault (for location, see figure 1). Black dashed lines are secondary faults. Inner DZ (yellow area) adjacent to the fault and outer DZ (grey area) boundary are estimated with cumulative frequency curve (see Appendix 1.4 for more details). b) Stereonet of silica filled fractures and all mineralized fractures (lower hemisphere projections). Red line: plane of the Têt fault; red star: pole of the Têt fault plane.

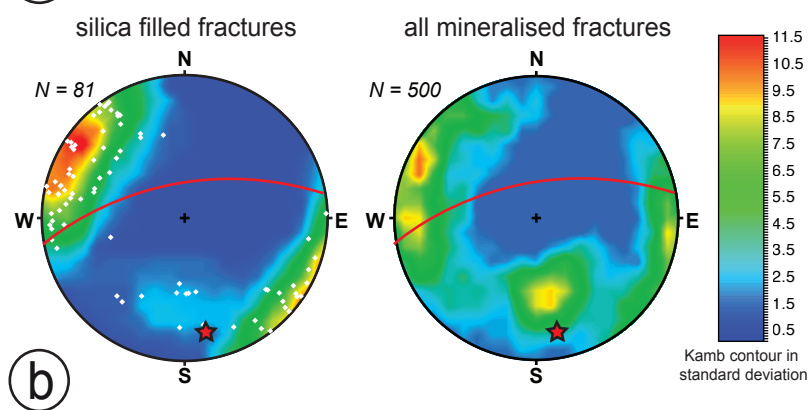
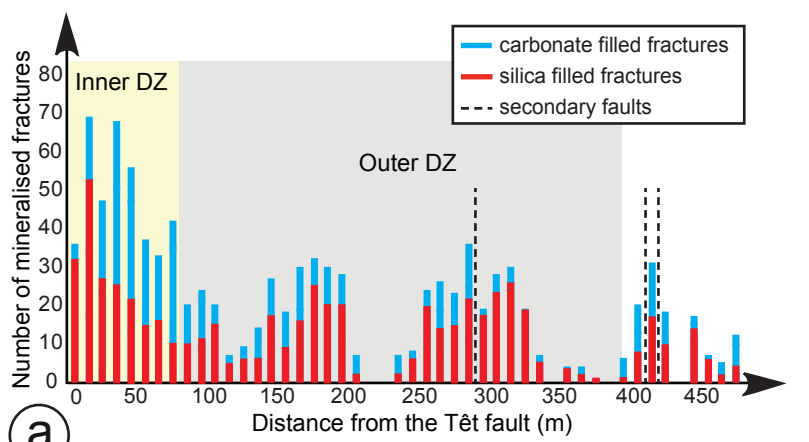
Figure 3. Synthetic cross section with sample location (stars). Samples TET5, TET6 and TET7 are projected (red stars) according to the normal fault distance. Near the fault, in the fault zone domain, the extent of the inner (yellow) and outer DZ (grey) is indicated.

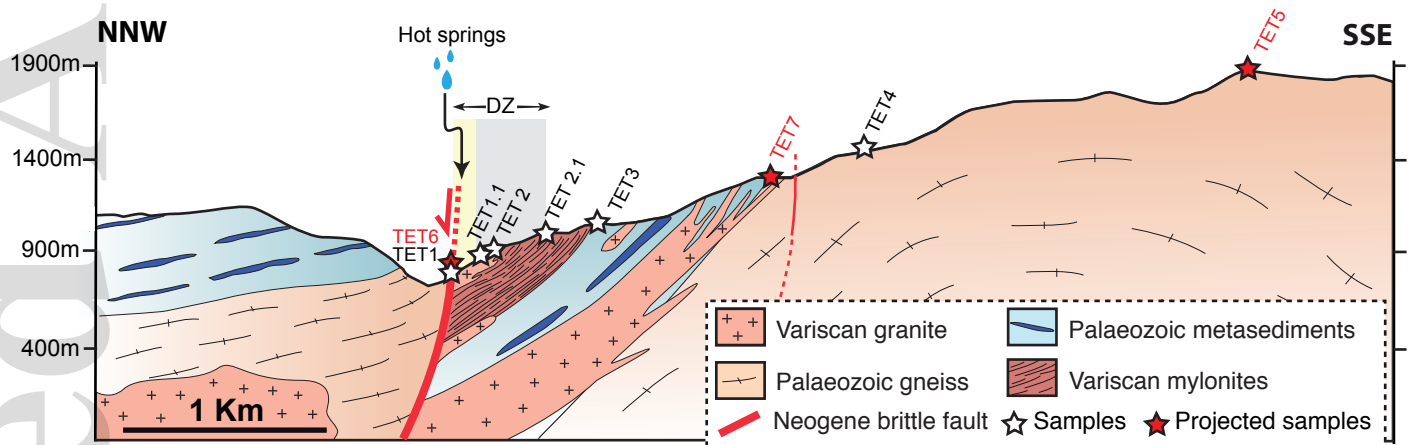
Figure 4. a) Graph of AHe ages as a function of the distance from the Têt fault. Circles are single grain AHe ages outside the DZ, squares for apatite grains in the outer DZ and triangles for apatite grains in the inner DZ (samples TET1 and TET6 are both adjacent to the fault). Fault zone domains are derived from Figure 2. b) Graph of elevation as a function of AHe ages with estimated denudation rate (dashed line). c) Chondrite normalized REE patterns for dated apatite grains. Black lines and circles correspond to the TET5 reference sample, squares represent samples in the outer DZ and triangles one sample in the inner DZ. Apatite single grains from the inner DZ show increased REE content compared to grains from the outer DZ that display reduced REE content according to reference sample TET5 from the Carança massif (for sample location, see Fig. 1).

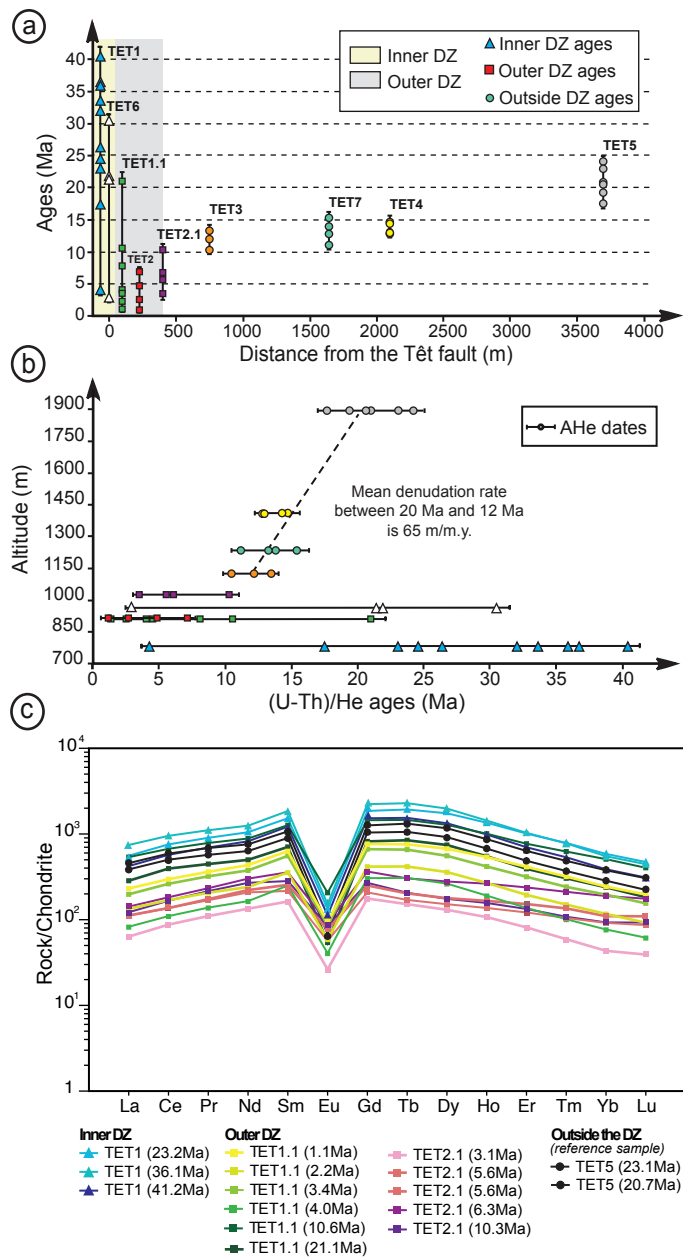
Figure 5. a) QTQt thermal modelling results (Gallagher, 2012) for the Têt fault footwall using AHe ages of samples TET3, TET4, TET5 and TET7 outside the damage zone, computed with the Gautheron et al. (2009) diffusion parameters. b) Graph of predicted AHe ages vs. observed AHe ages. 1:1 diagonal line corresponds to an ideal fit.

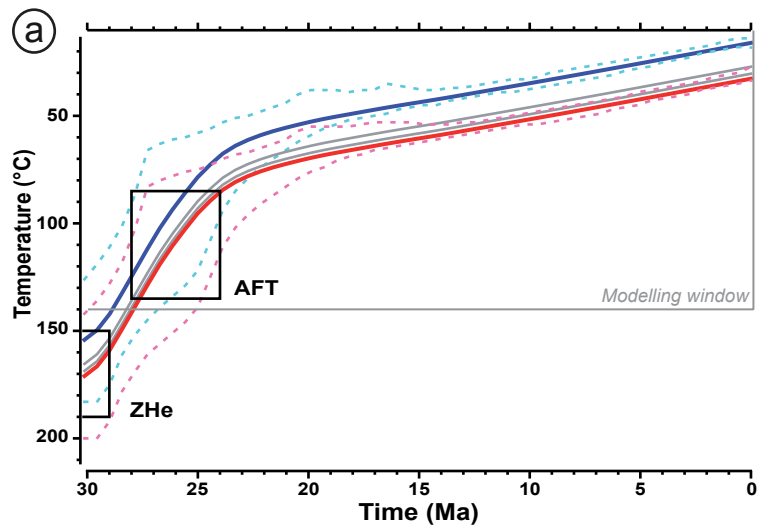
Figure 6. Isotopic data reported in a ternary U-Th-He diagram using HelioPlot (Vermeesch, 2010). Ellipses correspond to single grain analyses with associated errors. Three AHe age domains are distinguished imaging the various domains of fracturing, fluid activity and He mobility in the Têt fault footwall.











QTQt modelling of regional cooling using samples TET3,4,5 and 7 AFT et ZHe data from Maurel et al. (2008)

- T-t path for the uppermost sample (TET5)  
dashed lines correspond to 95% confidence interval
- T-t path for lowermost sample (TET3)  
dashed lines correspond to 95% confidence interval

